Title

Altered structural brain connectome in young adult fragile X premutation carriers

Journal

Human Brain Mapping, 35(9)

ISSN

1065-9471

Authors

Leow, Alex

Harvey, Danielle

Goodrich-Hunsaker, Naomi J

et al.

Publication Date

2014-09-01

DOI

10.1002/hbm.22491

Peer reviewed

◆ Human Brain Mapping 35:4518–4530 (2014) ◆

Altered Structural Brain Connectome in Young Adult Fragile X Premutation Carriers

Alex Leow,[1,2]* Danielle Harvey,[3,4] Naomi J. Goodrich-Hunsaker,[5] Johnson Gadelkarim,[1,6] Anand Kumar,[1] Liang Zhan,[7] Susan M. Rivera,[8] and Tony J. Simon[5]*

[1]Department of Psychiatry, University of Illinois at Chicago, Chicago, Illinois
[2]Department of Bioengineering, University of Illinois at Chicago, Chicago, Illinois, and Community Psychiatry, Sacramento, California
[3]Division of Biostatistics, School of Medicine, University of California, Davis, California
[4]Department of Public Health Sciences, School of Medicine, University of California, Davis, California
[5]MIND Institute and Department of Psychiatry and Behavioral Sciences, University of California, Davis, Sacramento, California
[6]Department of Electrical and Computer Engineering, University of Illinois at Chicago, Illinois
[7]LONI, Department of Neurology, University of California Los Angeles, Los Angeles, California
[8]MIND Institute, Department of Psychology, and University of California, Davis Center for Mind and Brain, Davis, California

Abstract: Fragile X premutation carriers (fXPC) are characterized by 55–200 CGG trinucleotide repeats in the 5′ untranslated region on the Xq27.3 site of the X chromosome. Clinically, they are associated with the fragile X-Associated Tremor/Ataxia Syndrome, a late-onset neurodegenerative disorder with diffuse white matter neuropathology. Here, we conducted first-ever graph theoretical network analyses in fXPCs using 30-direction diffusion-weighted magnetic resonance images acquired from 42 healthy controls aged 18–44 years (HC; 22 male and 20 female) and 46 fXPCs (16 male and 30 female). Globally, we found no differences between the fXPCs and HCs within each gender for all global graph theoretical measures. In male fXPCs, global efficiency was significantly negatively associated with the number of CGG repeats. For nodal measures, significant group differences were found between male fXPCs and male HCs in the right fusiform and the right ventral diencephalon (for nodal efficiency), and in the left hippocampus [for nodal clustering coefficient (CC)]. In female fXPCs, CC in the left superior parietal cortex correlated with counting performance in an enumeration task. *Hum Brain Mapp 35:4518–4530, 2014.* © 2014 Wiley Periodicals, Inc.

Key words: DTI; structural connectome; graph theory; fragile X; FXTAS; CGG

This article was published online on 27 February 2014. An error was subsequently identified. This notice is included in the online and print versions to indicate that both have been corrected 3 April 2014.

Contract grant sponsor: National Institute of Health (NIH); Contract grant numbers: NIA RL1 AG032119, NINDS RL1 NS062412, and NIDA TL1 DA024854; Contract grant sponsor: Roadmap Initiative grant; Contract grant number: UL1 DE019583; Contract grant sponsor: National Institute of Dental and Craniofacial Research (NIDCR)

Conflict of Interest: The authors declare that they have no competing interests.

*Correspondence to: Alex Leow, Psychiatric Institute, 1601 West Taylor Street, Room 584, Chicago, IL 60612. E-mail: alexfeuillet@gmail.com or Tony J. Simon, University of California, Davis MIND Institute, 2825 50th Street, Room 2341, Sacramento, CA 95817. E-mail: tjsimon@ucdavis.edu

Received for publication 18 October 2013; Revised 16 January 2014; Accepted 5 February 2014.

DOI 10.1002/hbm.22491

Published online 27 February 2014 in Wiley Online Library (wileyonlinelibrary.com).

INTRODUCTION

Fragile X syndrome (FXS) is the most common inherited form of mental retardation and the most prevalent known single-gene cause of autism in males [Schneider et al., 2009]. The fragile X mental retardation 1 gene (*FMR1*) is associated with CGG trinucleotide repeats in the 5′ untranslated region on the Xq27.3 site of the X chromosome [Verkerk et al., 1991]. Normally, unaffected individuals have fewer than 45 CGG repeats in *FMR1*. When the size of the CGG repeat exceeds 200 *FMR1* is silenced and the mutation is categorized as full, generating the FXS phenotype. If the expansion is between 55 and 200 repeats, then the individual is a fragile X premutation carrier (fXPC) [Garcia-Arocena and Hagerman, 2010; Hagerman and Hagerman, 2004]. Overall, it has been estimated that 1 in 260–813 males and 1 in 113–259 females in the population are fXPCs [Hagerman, 2008]. A major clinical consequence of the premutation allele is Fragile X-Associated Tremor/Ataxia Syndrome (FXTAS), a late-onset (usually 50–70 years old) neurodegenerative disorder that affects ~40% of male and 8–16% of female fXPCs [Jacquemont et al., 2004a,b]. Clinically, FXTAS is associated with tremors, gait ataxia, parkinsonism, and short-term memory and executive function impairments [Bourgeois et al., 2009].

In structural magnetic resonance images (MRI), FXTAS males in general show characteristic findings of diffuse signal changes in cerebellar white matter surrounding the dentate nuclei and in the middle cerebellar peduncles [Brunberg et al., 2002]. Neuropathological studies have reported prominent inclusion-bearing astrocytes in cerebral white matter, although intranuclear inclusions have been noted in both brain and spinal cord thus suggesting diffuse white matter involvement [Greco et al., 2006]. For female FXTAS patients, similar neuropathological changes of intranuclear neuronal and astrocytic inclusions were also reported in a small sample of five female fXPCs with possible FXTAS [Hagerman et al., 2004].

There have been several studies that probe white matter integrity across the spectrum of those affected by *FMR1* mutations with newer imaging techniques such as diffusion tensor imaging (DTI). Two related studies on male and female FXS [Barnea-Goraly et al., 2003; Haas et al., 2009] using DTI showed that relative to controls, young males with FXS had increased density of DTI reconstructed fibers in the left ventral frontostriatal pathway, while FXS females exhibited lower fractional anisotropy (FA) values in frontostriatal pathways and parietal sensory-motor tracts.

Hashimoto et al. [2011] used DTI to study male fXPCs with and without FXTAS syndrome versus healthy controls (a total sample of 71 male participants). There, the individuals with FXTAS showed significantly lower FA in multiple white matter tracts, including the middle cerebellar peduncle, superior cerebellar peduncle, cerebral peduncle, and the fornix and stria terminalis. Furthermore, regression analyses demonstrated a clear inverted U-shaped relationship between CGG-repeat size and axial and radial diffusivities in the middle cerebellar peduncle. In addition to CGG modulation in tract integrity, age-dependent effects have also been reported using a smaller sample in male fXPCs [Wang et al., 2012], where the authors reported that the premutation status was associated with a greater age-related white matter connectivity decline.

Even more subtle, yet significant, impairments in several domains involving spatial and numerical functioning have been reported in young, neurologically asymptomatic male and female adult fXPCs. Our own group, studying participants in the present sample, previously reported age- and CGG length-related impairment on an attentionally demanding enumeration task and on a spatial magnitude comparison task in 20–40 year old female fXPCs [Goodrich-Hunsaker et al., 2011a, Goodrich-Hunsaker et al., 2011b]. This was the case even though overall performance was not worse in the fXPC group and despite the fact that the psychomotor speed of the female fXPCs was quicker than that of the unaffected female controls of the same age [Goodrich-Hunsaker et al., 2011c]. By contrast, male fXPCS of the same age were not faster than healthy controls and did show significant group impairments on the same two tasks completed by the females but we did not find evidence of age- or CGG length modulations of functioning [Wong et al., 2012]. However, an fMRI study using a different magnitude estimation task with males and females from the same sample [Kim et al., 2013] did reveal reduced parietal activations that were CGG length-related, suggesting alterations in the neural substrate for magnitude processing in both genders.

Thus, it is possible that impairments in these functional domains might provide sensitive biomarkers for cognitive decline long before neurological symptoms emerge, especially if they can be linked to changes in neural networks known to underlie the main symptomatic features of the FXTAS spectrum in adult fXPCs.

Therefore, in this study, we employ a novel neuroimaging technique that uses state-of-the-art mathematics borrowed from graph-theory in order to characterize and analyze the complex properties of brain networks or "connectomes" [Rubinov and Sporns, 2010]. Such analyses provide quantitative assessment of brain connectomes by mathematically representing them as "graphs," which contain the nodes (gray matter) and the edges (white matter) connecting the nodes. Graph theoretical measures that characterize system properties can then be constructed; these metrics have most recently been shown to yield novel insight into the human brain's network properties, which can additionally be related to information such as clinical symptom severity [Bullmore and Sporns, 2009]; for an overview of these novel measures and their applications in neuroimaging, also refer to [Griffa et al., 2013; Wig et al., 2011; Xia and He, 2011].

This article represents the first ever connectome study using DTI-whole brain tractography based structural brain networks of young adult, neurologically asymptomatic,

TABLE I. Participant descriptive statistics and *FMR1* measures

	Female HC			Male HC			Female fXPC			Male fXPC		
	n	Mean (SD)	Range	*n*	Mean (SD)	Range	*n*	Mean (SD)	Range	*n*	Mean (SD)	Range
Age[a]	20	30.5 (7.1)	20.5–39.4	22	30.7 (7.1)	18.8–40.7	30	33.4 (5.6)	21.9–42.8	16	31.5 (6.4)	20.2–44.7
FSIQ[b]	15	110.9 (13.3)	89–129	16	117.5 (18.6)	85–148	22	117.5 (12.1)	97–144	12	117.1 (12.8)	94–136
CGG Repeat	17	30.1 (1.4)	28–33	15	29.1 (1.9)	24–33	30	94.4 (17.9)	67–141	14	89.4 (18.0)	55–118

[a]Main effect of group ($F = 1.07$, $P = 0.37$).
[b]Main effect of group ($F = 0.79$, $P = 0.50$).
FSIQ: Full scale IQ; SD: standard deviation.

fXPC, both male and female, compared with those from a sample of age and gender matched healthy control participants. Our primary interests are in characterizing differences, within each gender, between brain networks in relatively young and healthy adult fXPCs asymptomatic for FXTAS and unaffected controls. Secondary interests further include comparing networks between male and female fXPCs and exploring whether there is a fXPC-by-gender effect. To this end, we generated graph theoretical measures based on DTI-whole brain tractography, and then correlated them with behavioral or other clinical data, on both a global and nodal level.

We hypothesized that our findings would show altered organization of key brain networks in our male participants relative to those of the unaffected male controls, even though the male fXPCs did not manifest any neurological or other visible premonitory symptoms of FXTAS. Given the lower risk for FXTAS or related neurological symptoms in female fXPCs we did not expect to find such differences when their brains were compared with those of the unaffected female controls. By contrast, our studies of their cognitive performance on a range of tasks did reveal that, despite the absence of any clinical symptomology in the male and female fXPCs, they performed significantly worse in several tests compared to unaffected controls, and that in some cases their performance was correlated with age or CGG repeat length. Therefore, we hypothesized that changes in circuits involving subcortical motor pathways and in parietal magnitude, processing systems might correlate with our fine-grained behavioral data, possibly serving to identify potential biomarkers for those most at risk for neurocognitive decline.

METHODS

Participant Recruitment and Demographics

Descriptive statistics of age, full scale IQ score, and CGG repeat length are reported in Table I. Participants were 88 adults aged 18–44 years, including 42 healthy controls (HCs; 22 male and 20 female) and 46 fXPCs (16 male and 30 female). The mean age (± SD) for female HCs was 30.5 ± 7.1 years, for male HCs was 30.7 ± 7.1, for female fXPCs was 33.4 ± 5.6 years, and for male fXPCs was 31.5 ± 6.4 years. The three groups did not differ in age ($F = 1.07$, $P = 0.37$) or Full Scale IQ ($F = 0.79$, $P = 0.50$). Participants were recruited through the NeuroTherapeutics Research Institute (NTRI) at the Medical Investigation of Neurodevelopmental Disorders (MIND) Institute of the University of California, Davis Medical Center. This study was approved by the University of California Davis Institutional Review Board and conformed to institutional and federal guidelines for the protection of human participants. Written informed consent was obtained from all participants.

Psychological Assessment

All study participants completed an extensive battery of experimental tests of cognitive processing involving attention, executive function, spatial and temporal processing, some of whose results have been described elsewhere [Goodrich-Hunsaker et al., 2011a, b, c; Wong et al., 2012]. Global intellectual ability was measured either using the Wechsler Adult Intelligence Scale, third edition [Wechsler, 1997] or the Wechsler Abbreviated Scale of Intelligence [Wechsler, 1999]. IQ data were available for 15/20 female HCs, 16/22 male HCs, 22/30 female fXPCs, and 12/16 male fXPCs.

Molecular Analysis

Additionally, as previously described [Tassone et al., 2008], for all participants genomic DNA samples were obtained and extracted from peripheral blood leucocytes using standard methods (Puregene Kit; Gentra Inc., Valencia, CA). CGG Repeat sizes were determined using Southern blot and PCR amplification of genomic DNA.

MRI Acquisition

Diffusion weighted MRI of the participants were obtained using a Siemens Trio 3T scanner at the University of California, Davis Imaging Research Center. Seventy-two contiguous axial brain slices were collected with the following

parameters: 30 diffusion − weighted ($b = 700$ s/mm^2) and 1 ($b = 0$ s/mm$^{2)}$ nondiffusion weighted scan; field of view 243 mm; voxel size 1.9 × 1.9 × 1.9 mm; repetition time- = 11,900 ms; echo time = 92 ms. In addition, structural images were acquired with T1-weighted magnetization-prepared rapid gradient echo (MPRAGE). One sequence consisted of 208 contiguous sagittal slices with TR (repetition time) = 1,900 ms; TE (echo time) = 2.26 ms; in-plane resolution = 0.47 × 0.47 mm; slice thickness = 0.95 mm; flip angle = 9°; and a field of view of 207 and an acquisition matrix of 512 × 512. The second sequence consisted of 192 contiguous sagittal slices with TR (repetition time)- = 2,170 ms; TE (echo time) = 4.86 ms; in-plane resolution = 1 × 1 mm; slice thickness = 1 mm; flip angle = 7°; and a field of view of 192 and an acquisition matrix of 256 × 256.

Constructing Structural Brain Networks

Structural brain networks were generated using a pipeline, which integrates multiple image analysis techniques and has been described in detail elsewhere [GadElkarim et al., 2012; Leow et al., 2013]. Briefly, diffusion-weighted MR images were eddy current corrected using the automatic image registration tool embedded in DtiStudio software (http://www.mristudio.org) by registering all DW images to their corresponding b0 images with 12-parameter affine transformations. This was followed by the computation of diffusion tensors and deterministic tractography using the DtiStudio program (Fiber Assignment by Continuous Tracking or FACT algorithm; seeding at each voxel; maximum bending angle 60°; FA cut-off 0.15). High-resolution T1-weighted MPRAGE images were used to generate label maps using the Freesurfer software (http://surfer.nmr.mgh.harvard.edu). For all subjects, MPRAGE volumes were then registered to the corresponding b0 images using 12-parameter affine transformations, thus bringing label maps to each subject's individual DTI space. Weighted brain structural networks formed by the 87 Freesurfer-derived cortical, subcortical and brain stem gray matter regions were generated using an in-house program in MATLAB by counting the number of fibers connecting each pair of nodes. Mathematically, these structural networks were represented using 87 by 87 symmetric matrices or "graphs," on which graph theoretical analyses were performed (globally the groups did not differ in the total number of streamlines in the structural connectome: Male fXPC: 1,559 ± 224, Male HC: 1,653 ± 210; $P = 0.25$, Female fXPC: 1,777 ± 278, Female HC: 1,699 ± 238; $P = 0.30$).

Brief Summary of Graph Theoretical Measures

Here, we provide a brief explanation of the several graph theory metrics that are of relevance in this study. Various graph theoretical metrics have been proposed in order to quantify network organizational properties both at the global and the local levels [Bullmore and Sporns, 2009].

To mathematically compute these metrics, one may use either a binary or weighted approach. In the former, metrics are computed based on binarized matrices (i.e., the existence of an edge connecting two nodes depends on whether the fiber count exceeds a predetermined threshold). In this study we adopted the second, that is, weighted, approach where the weights of the connectivity matrix measure the connectivity strengths (the fiber counts) of graph edges. Basic binary graph theory network metrics include the degree of a node (the number of edges the node has connecting to others; the degree of a network is the mean degree of all nodes) and the density of a network (the total number of edges of a network divided by the maximum possible number of edges connecting the same number of nodes). More sophisticated measures defined for both binary and weighted graphs, including network efficiency, path length, and clustering coefficient (CC) can be calculated.

To briefly summarize these more sophisticated graph measures, we first need to construct the graph distance matrix, whose entries denote the shortest graph path lengths, or "graph distances," connecting node pairs. To this end, a transformation on the connectivity matrix that relates the connectivity edge strength to edge "length" is needed, such that higher fiber counts indicate shorter path lengths (usually the numerical inverse of fiber counts is used for this purpose, a practice we adopted in this study). Shortest path lengths are then constructed using the well-known Dijkstra algorithm [Dijkstra, 1959].

The longer the graph distance is between two nodes, the less efficient it is for information to transfer between them, and thus graph distances can be used to construct measures of network integration. Calculated by averaging the graph distances between all pairs of nodes, the characteristic path length or CPL measures how efficiently information can be transferred within the whole network, and is thus considered a measure of global network integration (node-level path length is defined similarly by averaging the shortest paths connecting this node to all other nodes in the entire network). Networks with longer CPL exhibit information flows that are slower (due to the longer distance needed to travel between nodes) compared to those with shorter CPL, and are thus less efficient. A related global metric, the global efficiency (Eglob), calculates the average inverse graph distances between all pairs of nodes. Thus, both higher Eglob values and lower CPL values indicate more efficient network integration [Bullmore and Sporns, 2009].

As a measure of network clustering or segregation, the weighted CC of a node is defined as the degree to which this node and its immediate neighbors are interconnected among themselves (nodes with high CC thus form locally interconnected clusters). The CC of the whole network averages CC across all nodes. It is noted that brain

networks, like most naturally occurring networks, exhibit a "small world" property such that they consist of clusters of segregated nodes that locally interact with one another to form a "module," while globally these clusters remain efficiently integrated (mathematically speaking, small-world networks have similar shortest path lengths but higher CCs relative to random networks with the same density and number of nodes).

Lastly, we also computed the normalized global path length (lambda) and the normalized global CC (gamma), both normalized against random networks with the same density and number of fibers.

Statistical Analysis

The fXPCs were split into two groups based on gender, because many differences have been observed between male and female fXPCs in other measures. As our primary interests are in within-gender analyses between fxPCs and HCs, regional brain volumes were not normalized to each individual's total brain volume, which tends to differ between genders. Typical controls were also split by gender to assess differences in the same way. Analysis of variance (volumetric measures) or Kruskal-Wallis tests (network measures) were used as a global test to compare across the four groups, depending on the skewed nature of many of the distributions. Within a measure, a Bonferroni correction (0.05/# regions) was used to identify regions with a significant group difference. For the global measures, multiple comparisons were conducted across each variable. If the four-group comparison was significant, post-hoc pairwise comparisons using the Welch two-sample t-test (volumetric measures) or Wilcoxon rank sum test (network measures) were performed to determine specifically which groups were different. False Discovery Rate (FDR) was then applied to the two group comparisons across significant global network metrics, or regions (in the case of volumetric measures or local network metrics). Only results from regions that remained significant for a four-group comparison after the Bonferonni correction are presented with notations for the regions that had FDR-adjusted significant two-group differences. To further explore implications of the DTI-based structural connectome in the fXPCs, within-gender Spearman rank correlations were assessed between global measures and age and CGG repeat. Within-gender associations in fXPCs between psychometric task performance and node-level measures (local efficiency, local CC, and local path length) in regions hypothesized to be involved during simple reaction tasks (thalamus, pre-/post-/para- central gyri, posterior cingulate, and the cerebellum and brainstem) or Enumeration or Magnitude Comparison tasks (precuneus, superior and inferior parietal lobules, and cerebellum) were assessed using linear regression. Similar to the two-group differences, FDR was used to adjust for multiple comparisons across the different regions and tasks. Further models included CGG repeat length in order to account for previously observed associations between genetic dosage and task performance. All analyses were conducted in R, Version 2.15.0

RESULTS

Volumetric Measures at the Node Level

The volume for each FSL-generated gray matter ROI was measured by counting the number of voxels for every region (to translate the volume size into mm^3, the number of voxels need to be multiplied by $1.89 \times 1.89 \times 1.9 = 6.787$ mm^3). As expected, there were significant gender differences in volumetric measures for each diagnostic group (Table II). Within each gender, volumetric differences between fXPCs and typical controls were of particular interest. Our data indicated that in males, fXPCs had smaller brain stem volumes than HCs ($t(35.3) = 4.02$, $p < 0.05$ after FDR correction). By contrast, female fXPCs had larger ROI volumes for the right superior temporal gyrus, right superior parietal gyrus, and right posterior cingulate ($t(44.1) = -2.24$, $t(30.1) = -2.40$, $t(43.7) = -2.48$, respectively; $P < 0.05$ after FDR correction for each) than female HCs. (Table II presents all significant differences in brain volume at the node level. However, since volumes were not normalized to total brain size within each gender, between gender significance values may be affected by differences in overall brain size).

Global Graph Theoretical Measures

Group level results

Figure 1 visualizes the generated mean structural networks for all four groups; there were no statistical differences in the number of reconstructed fiber tracts or streamlines (the mean number of streamlines of a network is also referred to as the strength) across the four groups ($P = 0.09$). For global graph theoretical measures, within each gender we found no differences between the fXPCs and HCs. However, between males and females several global measures including CC and gamma (normalized CC) exhibited group differences. Females had lower gamma and CC relative to males, regardless of their diagnostic group (the remaining global graph theoretical measures showed no differences; see Table III).

Correlation results

There were no significant associations between age and any of the global measures. However, in the male fXPCs, global efficiency significantly negatively correlated with the number of CGG repeats ($n = 14$, $r = -0.63$, $P = 0.02$, Fig. 2), suggesting that increased genetic dosage (independent of age) significantly negatively affected global network integration. In female fXPCs, this correlation

TABLE II. Volumetric differences (in voxels; one voxel = 6.787 mm^3) at the node level

	fXPC male		HC male		fXPC female		HC female		
Region, Hemisphere (R/L)	Mean (SD)	Median	Mean (SD)	Median	Mean (SD)	Median	Mean (SD)	Median	*P*-value
Frontal Lobe									
Insula, R	1,194 (125)	1,184	1,210 (122)	1,205	1,074 (133)[a,b]	1,095	1,070 (138)[a,b]	1,016	<0.001
Insula, L	1,191 (90)	1,181	1,150 (91)	1,152	1,058 (116)[a,b]	1,053	1,019 (117)[a,b]	1,020	<0.001
Parietal Lobe									
Superior parietal cortex, R	2,058 (287)	2,044	2,163 (253)	2,128	1,998 (195)[a,c]	2,000	1,819 (293)[a,b]	1,890	<0.001
Inferior parietal cortex, R	2,530 (345)	2,500	2,623 (319)	2,606	2,267 (235)[a,b]	2,264	2,168 (242)[a,b]	2,210	<0.001
Inferior parietal cortex, L	2,086 (249)	2,174	2,069 (265)	2,030	1,840 (198)[a,b]	1,857	1,776 (250)[a,b]	1,776	<0.001
Precuneus cortex, R	1,696 (168)	1,704	1,675 (219)	1,693	1,486 (174)[a,b]	1,489	1,416 (254)[a,b]	1,351	<0.001
Precuneus cortex, L	1,536 (125)	1,505	1,627 (178)	1,629	1,448 (149)[a]	1,446	1,387 (195)[a,b]	1,339	<0.001
Temporal Lobe									
Superior temporal gyrus, R	1,916 (232)	1,895	1,968 (211)	1,970	1,807 (226)[a,c]	1,800	1,670 (201)[a,b]	1,685	<0.001
Superior temporal gyrus, L	2,011 (240)	1,998	2,070 (229)	2,074	1,855 (214)[a]	1,844	1,790 (239)[a,b]	1,817	<0.001
Middle temporal gyrus, R	1,990 (288)	2,000	1,999 (277)	2,064	1,758 (212)[a,b]	1,755	1,743 (251)[a,b]	1,774	<0.001
Middle temporal gyrus, L	1,856 (231)	1,848	1,799 (291)	1,763	1,579 (163)[a,b]	1,582	1,597 (187)[a,b]	1,636	<0.001
Inferior temporal gyrus, L	1,674 (228)	1,670	1,625 (226)	1,632	1,476 (197)[a,b]	1,554	1,353 (298)[a,b]	1,365	<0.001
Entorhinal cortex, R	338 (61)	324	312 (58)	329	264 (42)[a,b]	256	255 (50)[a,b]	253	<0.001
Occipital Lobe									
Lateral occipital, L	1,793 (186)	1,829	1,716 (226)	1,688	1,512 (244)[a,b]	1,502	1,486 (298)[a,b]	1,562	<0.001
Lateral occipital, R	1,748 (244)	1,705	1,658 (278)	1,660	1,474 (227)[a,b]	1,514	1,401 (288)[a,b]	1,470	<0.001
Cuneus, L	473 (54)	473	462 (74)	440	413 (62)[a,b]	417	394 (48)[a,b]	406	<0.001
Cingulate Cortex									
Posterior-cingulate cortex, R	540 (78)	543	518 (90)	509	480 (79)[b,c]	469	427 (72)[a,b]	424	<0.001
Isthmus-cingulate cortex, R	390 (67)	383	377 (62)	375	342 (56)[b]	338	311 (43)[a,b]	319	<0.001
Subcortical									
Amygdala, L	253 (30)	252	262 (26)	262	229 (34)[a,b]	233	225 (27)[a,b]	223	<0.001
Caudate, R	693 (87)	693	736 (109)	714	653 (87)[a]	655	610 (68)[a,b]	599	<0.001
Caudate, L	682 (78)	693	719 (87)	701	638 (80)[a]	640	600 (57)[a,b]	607	<0.001
Pallidum, R	297 (51)	283	323 (65)	320	258 (33)[a,b]	254	262 (30)[a,b]	258	<0.001
Pallidum, L	353 (50)	337	393 (59)	394	327 (35)[a]	333	322 (33)[a]	322	<0.001
Thalamus, R	1,446 (122)	1,462	1,542 (174)	1,510	1,324 (143)[a,b]	1,322	1,286 (122)[a,b]	1,255	<0.001
Thalamus, L	1,414 (72)	1,420	1,509 (196)	1,504	1,298 (133)[a,b]	1,280	1,286 (119)[a,b]	1,286	<0.001
Ventral diencephalon, R	734 (65)	712	763 (61)	766	697 (67)[a]	695	682 (50)[a,b]	684	<0.001
Brainstem	3,151 (230)[a]	3,089	3,543 (369)	3,619	3,134 (339)[a]	3,092	2,900 (506)[a]	2,933	<0.001

[a]Significantly different from male HC.
[b]Significantly different from male fXPC.
[c]Significantly different from female HC.

remained negative although did not reach statistical significance ($n = 30$, $r = -0.10$, $P = 0.58$). There were no significant associations in the female fXPCs.

Node Level Graph Measures

Group level results

For node level graph measures, significant group differences were found between male fXPCs and male HCs for local efficiency in the right fusiform and the right ventral diencephalon. For node-level CC male fXPCs had lower values in the left hippocampus (see Table IV). For females, there were by contrast no significant group differences compared to female HCs for any node-level graph theoretical measures in female fXPCs (see Tables IV and V).

Correlation results

In several brain regions, correlations between performance on our cognitive task battery and network values produced significant values, indicating the functional implications of these brain changes. These are depicted on the surface rendering in Figure 3A. In female fXPCs, CC in the left superior parietal cortex correlated with response time in the counting component of the Enumeration task ($r = 0.75$, $P < 0.001$, see region 1 in Fig. 3A,B). The indication that higher CC was associated with a greater increase in response time in response to increasing complexity of the

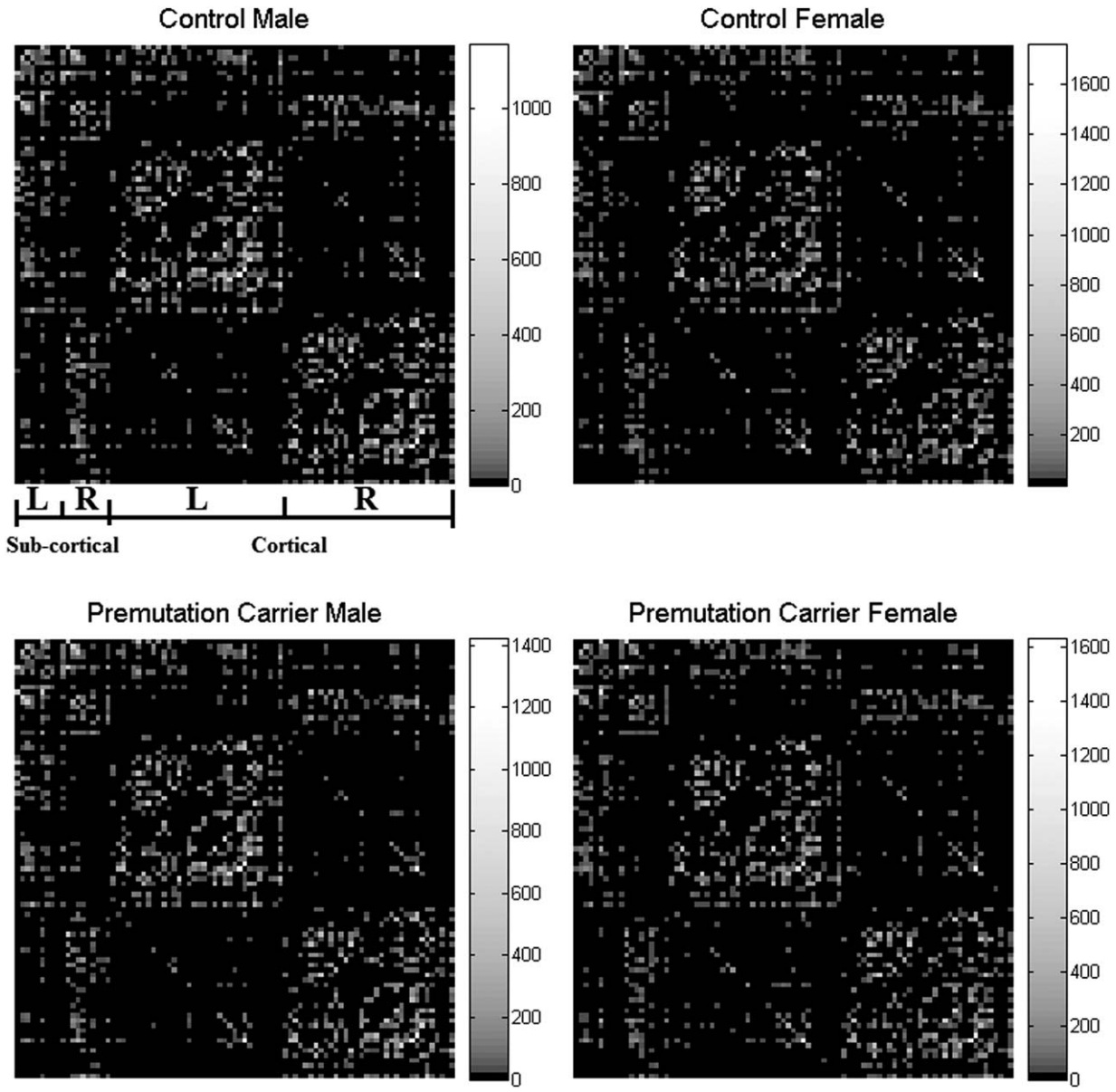

Figure 1.
This figure visualizes the mean structural brain networks for all 4 groups in this study.

task suggests that this critical cortical region was excessively localized relative to the global network in female carriers, thus compromising its role in communicating effectively with other critical neural regions of the circuit. This association remained statistically significant even after accounting for CGG repeat size ($t = 6.0$, $P < 0.005$). (It is worth noting that this result is consistent with the involvement of parietal regions in numerical and attentional control functions that are critical components of this task.)

Several other relationships that were consistent with our hypotheses did not survive the FDR criteria for statistical significance. In particular, nodal CC showed a positive relationship in the left inferior parietal cortex ($r = 0.52$, $P = 0.006$) with response time in the counting component of the Enumeration task (Region 2 in Fig. 3A) and in the left precuneus with response time in the subitizing component of the Enumeration task ($r = 0.47$, $P = 0.01$; see region 3 in Fig. 3A). As above these results indicate that higher CCs (i.e., stronger local segregation) were associated with longer response times. In addition, nodal path length showed a positive association with oral motor reaction time in the right paracentral gyrus ($r = 0.44$, $P = 0.02$),

TABLE III. Global graph theoretical measures

	fXPC male		HC male		fXPC female		HC female		
Measure	Mean (SD)	Median	Mean (SD)	Median	Mean (SD)	Median	Mean (SD)	Median	*P*-value
Strength (mean fiber count)	1559 (224)	1548	1653 (210)	1708	1777 (278)	1750	1699 (238)	1638	0.09
Normalized CC	2.3 (0.2)	2.3	2.3 (0.2)	2.3	2.0 (0.3)[a,b]	1.9	2.0 (0.3)[a,b]	1.9	<0.001
Clustering coefficient	28.5 (3.5)	28.9	28.8 (2.9)	29.2	25.1 (2.9)[a,b]	25.1	24.8 (4.1)[a,b]	23.6	<0.001
Normalized path length	1.3 (0.1)	1.3	1.4 (0.3)	1.3	1.3 (0.1)	1.3	1.3 (0.1)	1.3	0.1
Path length	0.18 (0.003)	0.018	0.018 (0.002)	0.017	0.019 (0.006)	0.017	0.018 (0.002)	0.018	0.7
Global efficiency	84.1 (10.9)	81.3	87.5 (10.0)	89.9	88.6 (13.2)	87.9	86.5 (11.6)	83.6	0.6

[a]Significantly different from male HC.
[b]Significantly different from male fXPC.

relating longer graph distance in this region (needed to reach other nodes in the graph) with longer reaction times (Region 5 in Fig. 3A). Lastly, there was a trend toward a negative association between nodal or local efficiency and manual motor reaction time in the brainstem ($r = -0.44$, $P = 0.02$; the higher the nodal efficiency in the brain stem, the shorter the reaction time; Region 4 in Fig. 3A).

In male fXPCs, there were no significant associations between nodal measures and task performance. However, since the sample size for this group was much smaller ($n = 16$), we believe the lack of significance in any of the correlations was more a consequence of reduced power than the lack of any relationships, especially because males are generally more heavily impacted than females.

DISCUSSION

In this article, we presented the first ever study on the brain connectome of fXPC, both male and female, relative to their age-equivalent healthy controls. We sought to achieve several goals with our analyses. One was to determine whether this method produces results that are consistent with, and/or complementary to the small but growing body of findings of neural anomalies in these groups. This is of particular interest because, unlike previous methods, the current technique is able to study, on a system level, the global interaction between the gray matter nodes and the white matter connections of the networks. A second goal was to exploit the integrative nature, in a system organizational context, of the connectome approach to see if our results might give any indication that this method could be used to detect biomarkers of disease risk earlier and more completely than is feasible for other methods, such that progression towards clinical manifestations as well as targets for and approaches to preventive intervention can be better understood.

Our key findings are summarized as follows. First, we found that, relative to unaffected male controls, young adult males fXPCs had reduced brainstem volumes, which is consistent with findings reported in older male permutation carriers. By contrast, relative to unaffected female controls, young adults female fXPCs had larger right superior temporal gyrus, right superior parietal gyrus, and right posterior cingulate volumes. These appear to be novel findings, and may suggest the presence of compensatory mechanisms in female (but not in male) related to the previously reported finding of faster psychomotor speed in female fXPCs than that of the unaffected female controls of the same age [Goodrich-Hunsaker et al., 2011c].

In terms of network characteristics, although no global differences were found between fXPCs and HCs, correlation analyses showed that global efficiency significantly negatively correlated with genetic dosage, as measured by CGG repeat length, in male fXPCs (and we found a negative but non-significant correlation in the female group). It

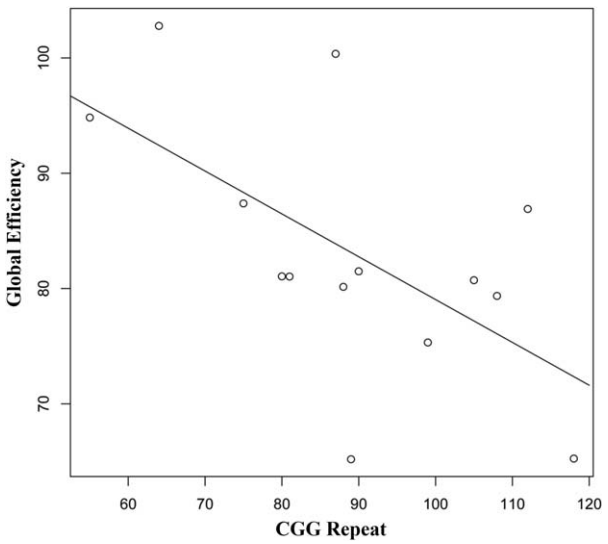

Figure 2.
Association between global efficiency and CGG repeat in male fXPCs ($n = 14$, $r = -0.63$, $P = 0.02$).

TABLE IV. Node level graph theoretical measures with significant group differences within males

Measure / Region	fXPC male		HC male		fXPC female		HC female		
	Mean (SD)	Median	Mean (SD)	Median	Mean (SD)	Median	Mean (SD)	Median	*P*-value
Local efficiency									
Fusiform, R	0.15 (0.03)[a]	0.15	0.20 (0.04)	0.20	0.24 (0.07)[a,b]	0.24	0.26 (0.06)[a,b]	0.26	<0.001
Ventral diencephalon, R	0.22 (0.03)[a]	0.22	0.24 (0.03)	0.24	0.29 (0.06)[a,b]	0.30	0.29 (0.07)[a,b]	0.31	<0.001
Local CC									
Hippocampus, L	19.3 (3.2)[a]	18.8	21.7 (2.9)	20.9	16.1 (4.3)[a,b]	15.1	17.3 (6.5)[a,b]	15.0	<0.001

[a]Significantly different from male HC.
[b]Significantly different from male fXPC.

should also be noted this CGG modulation effect is similar to the age effect on network efficiency (global efficiency for example, has been shown to decrease across the life span in a connectome study using interregional correlations between gray matter volumes [Zhu et al., 2012], thus providing an initial finding that links premutation dosage directly to neurodegenerative brain changes that are consistent with amplified effects of normal aging. Moreover, if we compare the −0.41 correlation between age and global efficiency reported in a recent study on structural brain networks in older participants processed using the same image processing pipeline [Ajilore et al., 2014] to our correlation of −0.63 between CGG repeat length in males, our findings suggest that increased CGG dosage in males represents an effective increase of ∼1.5 years per extra CGG repeat of "brain aging" as measured in terms of decreasing efficiency. The negative, but very small (−0.1), value of this correlation in females suggests that CGG repeat length alone does not contribute any significant risk, over aging alone, of neural aging. While unrelated to overall brain volumes, such a result is at very least, consistent with the very different trajectories in neurodegeneration seen in males and females as they age. These findings appear to satisfy our second goal, which was to exploit the integrative, system organizational nature of the connectome approach to seek to identify biomarkers of disease risk earlier and more completely than is feasible for other methods. Here, it appears that the negative global efficiency/CGG length correlation may prove to be an effective marker of "brain aging" that can be detected in apparently healthy, nonsymptomatic fXPCs. Such correlations were significant in our 20–40 year old male, and showed the same trend in young adult female fXPCs. If more sensitive measures of "genetic dosage" than CGG length become available then this relationship might prove to be an effective risk marker that could be detected long before any symptoms occur. This possible relationship urgently needs to be explored in a larger sample.

The patterns of relations in our global analyses of a lack of statistical differences between groups coupled with positive CGG modulation effect merit further discussion. First, the fact that our participants of this study were healthy young adults with no clinical symptoms beyond their carrier status may itself explain why we found no group differences in our global analyses. However, our significant correlation results support our proposal that cognitive function and clinical data along with connectome patterns are likely to better characterize underlying brain pathophysiology than diagnostic categories or gender alone. Categorical diagnostic constructs such as the fragile X premutation-carrying status (whose definition relies on a binary determination based on the participant's CGG repeat), may not capture the overlapping and continuously varying endophenotypes and phenotypes as well as a continuous variable such as the actual repeats of a participant's CGG. The lack of significant group differences on the global level also may be partly due to the relatively narrow age range and fairly small sample size of our dataset. Also, the fact that our diffusion-weighted MR imaging data were acquired using a reasonable angular resolution (30 directions), but without the advantage of, the now more common, very high angular resolution, may have reduced our power to detect small group differences.

However, at the node-level, several important results emerged. Reduced local efficiency (i.e., lower local network integration) in male fXPCs in the right fusiform and diencephalon appear to be consistent with oculomotor and visual processing changes evident in both FXS and the later occurring FXTAS phenotype [Kogan et al., 2004; Sulkowski and Kaufman, 2008]. Lower local CC (the degree to which neighboring nodes are interconnected) in the left hippocampus in male fXPCs relative to controls is consistent with the affective and cognitive differences that they manifest. While the translational implications of the directionality of this finding needs to be further studied in a future sample, such an involvement is consistent with several recent studies investigating a range of cognitive functions, including spatial processing, [Hocking et al., 2012; MacLeod et al., 2010; Wong et al., 2012] that have been theorized to be associated with hippocampus [Koldewyn et al., 2008; Wang et al., 2012] and with its role in affective processing by the limbic system [Jacquemont et al., 2004a,b; Hessl et al., 2007].

TABLE V. Node level graph theoretical measures with significant 4-group differences

Measure Region, Hemisphere (R/L)	fXPC male		HC male		fXPC female		HC female		
	Mean (SD)	Median	Mean (SD)	Median	Mean (SD)	Median	Mean (SD)	Median	*P*-value
Local CC									
Frontal Lobe									
Rostral middle frontal gyrus, R	53.4 (21.4)	50.0	50.6 (19.8)	48.3	36.1 (17.6)[a,b]	31.0	28.6 (15.7)[a,b]	24.9	<0.001
Rostral middle frontal gyrus, L	54.4 (16.0)	53.2	55.6 (25.3)	51.1	39.8 (21.8)[a,b]	32.4	35.5 (16.5)[a,b]	30.7	<0.001
Pars orbitalis, R	46.2 (12.4)	42.3	47.3 (16.7)	44.6	26.7 (12.6)[a,b]	24.0	30.9 (18.1)[a,b]	24.5	<0.001
Pars triangularis, R	51.8 (15.2)	50.0	47.0 (12.7)	46.6	32.3 (16.4)[a,b]	27.9	30.5 (16.8)[a,b]	22.6	<0.001
Pars triangularis, L	53.5 (16.6)	53.6	48.0 (13.7)	49.5	35.0 (19.2)[a,b]	28.7	32.5 (21.6)[a,b]	22.8	<0.001
Parietal Lobe									
Superior parietal cortex, L	31.3 (9.0)	29.5	33.1 (7.6)	32.8	25.0 (8.2)[a,b]	22.2	24.1 (8.0)[a,b]	21.2	<0.001
Precuneus cortex, R	26.6 (6.9)	26.2	27.2 (8.5)	26.1	19.3 (6.8)[a,b]	16.2	18.7 (6.2)[a,b]	16.5	<0.001
Precuneus cortex, L	24.0 (6.8)	24.9	25.5 (5.7)	25.4	19.6 (5.5)[a]	17.9	18.0 (5.4)[a,b]	16.1	<0.001
Temporal Lobe									
Temporal pole, R	36.1 (14.8)	33.6	29.5 (8.0)	27.1	22.4 (7.3)[a,b]	21.3	25.5 (9.2)[b]	23.3	<0.001
Temporal pole, L	34.3 (12.6)	33.9	35.2 (9.8)	34.5	25.2 (11.3)[a,b]	22.1	21.3 (7.4)[a,b]	20.1	<0.001
Subcortical									
Amygdala, R	22.6 (4.8)	22.0	20.5 (4.8)	19.5	15.6 (4.3)[a,b]	14.0	15.1 (5.8)[a,b]	13.1	<0.001
Hippocampus, R	22.9 (4.7)	22.9	23.0 (5.2)	21.8	14.7 (3.0)[a,b]	14.9	16.9 (6.7)[a,b]	14.4	<0.001
Hippocampus, L	19.3 (3.2)[a]	18.8	21.7 (2.9)	20.9	16.1 (4.3)[a,b]	15.1	17.3 (6.5)[a,b]	15.0	<0.001
Caudate, R	21.7 (4.7)	21.2	21.9 (4.9)	22.0	16.8 (3.9)[a,b]	16.3	17.6 (5.3)[a,b]	15.2	<0.001
Thalamus, R	21.4 (4.2)	20.6	23.2 (4.6)	21.9	17.4 (2.8)[a,b]	16.9	16.9 (4.3)[a,b]	15.3	<0.001
Thalamus, L	23.2 (3.9)	22.8	22.8 (4.4)	23.3	19.4 (4.2)[a,b]	19.2	18.0 (4.0)[a,b]	17.2	<0.001
Ventral diencephalon, R	19.5 (3.9)	19.7	20.7 (2.9)	21.2	15.4 (4.2)[a,b]	14.9	15.7 (3.6)[a,b]	14.7	<0.001
Local efficiency									
Frontal Lobe									
Pars triangularis, R	0.14 (0.07)	0.13	0.13 (0.07)	0.10	0.23 (0.09)[a,b]	0.24	0.22 (0.10)[a,b]	0.22	<0.001
Pars triangularis, L	0.14 (0.08)	0.11	0.14 (0.05)	0.13	0.22 (0.10)[a,b]	0.24	0.26 (0.09)[a,b]	0.29	<0.001
Pars orbitalis, R	0.09 (0.04)	0.09	0.09 (0.07)	0.07	0.19 (0.09)[a,b]	0.18	0.16 (0.09)[a,b]	0.16	<0.001
Medial orbitofrontal gyrus, R	0.21 (0.05)	0.20	0.19 (0.06)	0.18	0.26 (0.08)[a,b]	0.26	0.27 (0.06)[a,b]	0.28	<0.001
Medial orbitofrontal gyrus, L	0.19 (0.05)	0.17	0.20 (0.05)	0.20	0.26 (0.07)[a,b]	0.27	0.27 (0.07)[a,b]	0.28	<0.001
Insula, R	0.20 (0.04)	0.20	0.22 (0.04)	0.21	0.28 (0.06)[a,b]	0.27	0.27 (0.07)[a,b]	0.28	<0.001
Parietal Lobe									
Superior parietal cortex, R	0.16 (0.06)	0.14	0.17 (0.06)	0.18	0.28 (0.07)[a,b]	0.28	0.26 (0.07)[a,b]	0.28	<0.001
Superior parietal cortex, L	0.18 (0.06)	0.19	0.18 (0.06)	0.17	0.28 (0.07)[a,b]	0.29	0.27 (0.08)[a,b]	0.29	<0.001
Inferior parietal cortex, R	0.14 (0.06)	0.13	0.17 (0.06)	0.17	0.24 (0.07)[a,b]	0.26	0.23 (0.08)[a,b]	0.23	<0.001
Inferior parietal cortex, L	0.18 (0.07)	0.19	0.16 (0.05)	0.14	0.27 (0.08)[a,b]	0.29	0.26 (0.08)[a,b]	0.29	<0.001
Postcentral gyrus, R	0.17 (0.08)	0.16	0.18 (0.05)	0.18	0.23 (0.05)[a,b]	0.23	0.24 (0.06)[a,b]	0.25	<0.001
Precuneus, R	0.22 (0.07)	0.21	0.21 (0.04)	0.22	0.30 (0.06)[a,b]	0.28	0.27 (0.07)[a,b]	0.28	<0.001
Precuneus, L	0.21 (0.06)	0.20	0.21 (0.04)	0.21	0.29 (0.06)[a,b]	0.29	0.27 (0.07)[a,b]	0.28	<0.001
Temporal Lobe									
Superior temporal gyrus, R	0.16 (0.05)	0.17	0.18 (0.05)	0.18	0.24 (0.06)[a,b]	0.24	0.23 (0.07)[a,b]	0.22	<0.001
Superior temporal gyrus, L	0.22 (0.04)	0.21	0.20 (0.05)	0.20	0.27 (0.07)[a,b]	0.28	0.26 (0.07)[a]	0.27	<0.001
Middle temporal gyrus, R	0.13 (0.05)	0.12	0.15 (0.05)	0.15	0.22 (0.07)[a,b]	0.21	0.20 (0.07)[a,b]	0.19	<0.001
Inferior temporal gyrus, R	0.13 (0.03)	0.12	0.16 (0.05)	0.16	0.23 (0.07)[a,b]	0.23	0.20 (0.07)[b]	0.19	<0.001
Fusiform gyrus, R	0.15 (0.03)[a]	0.15	0.20 (0.04)	0.20	0.24 (0.07)[a,b]	0.24	0.26 (0.06)[a,b]	0.26	<0.001
Entorhinal cortex, R	0.13 (0.04)	0.12	0.15 (0.05)	0.15	0.22 (0.08)[a,b]	0.21	0.21 (0.08)[a,b]	0.21	<0.001
Temporal pole, R	0.12 (0.06)	0.11	0.14 (0.07)	0.13	0.22 (0.08)[a,b]	0.23	0.21 (0.08)[a,b]	0.21	<0.001
Parahippocampal gyrus, R	0.11 (0.04)	0.11	0.14 (0.04)	0.13	0.18 (0.07)[b]	0.17	0.19 (0.05)[a,b]	0.19	<0.001
Occipital Lobe									
Lateral occipital, L	0.16 (0.08)	0.17	0.16 (0.05)	0.15	0.26 (0.07)[a,b]	0.28	0.25 (0.06)[a,b]	0.27	<0.001
Lateral occipital, R	0.16 (0.05)	0.16	0.15 (0.06)	0.14	0.25 (0.08)[a,b]	0.26	0.24 (0.09)[a,b]	0.26	<0.001
Lingual, L	0.19 (0.07)	0.20	0.18 (0.05)	0.18	0.27 (0.07)[a,b]	0.28	0.27 (0.07)[a,b]	0.30	<0.001
Lingual, R	0.18 (0.05)	0.17	0.19 (0.05)	0.20	0.29 (0.07)[a,b]	0.30	0.26 (0.08)[a,b]	0.27	<0.001
Pericalcerine, L	0.14 (0.06)	0.12	0.14 (0.06)	0.14	0.24 (0.09)[a,b]	0.26	0.24 (0.09)[a,b]	0.27	<0.001

TABLE V. (continued).

Measure Region, Hemisphere (R/L)	fXPC male Mean (SD)	 Median	HC male Mean (SD)	 Median	fXPC female Mean (SD)	 Median	HC female Mean (SD)	 Median	*P*-value
Pericalcerine, R	0.14 (0.06)	0.14	0.17 (0.07)	0.18	0.25 (0.09)[a,b]	0.26	0.22 (0.08)[b]	0.23	<0.001
Subcortical									
Amygdala, R	0.14 (0.05)	0.15	0.16 (0.05)	0.15	0.23 (0.07)[a,b]	0.23	0.23 (0.08)[a,b]	0.25	<0.001
Hippocampus, R	0.21 (0.03)	0.21	0.23 (0.04)	0.23	0.29 (0.06)[a,b]	0.29	0.30 (0.05)[a,b]	0.31	<0.001
Hippocampus, L	0.25 (0.04)	0.25	0.23 (0.03)	0.24	0.29 (0.06)[a,b]	0.31	0.29 (0.07)[a,b]	0.33	<0.001
Putamen, R	0.23 (0.05)	0.23	0.23 (0.05)	0.22	0.29 (0.06)[a,b]	0.29	0.29 (0.06)[a,b]	0.31	<0.001
Thalamus, R	0.25 (0.05)	0.25	0.26 (0.03)	0.25	0.31 (0.05)[a,b]	0.30	0.30 (0.06)[a,b]	0.32	<0.001
Thalamus, L	0.26 (0.04)	0.26	0.25 (0.03)	0.26	0.31 (0.05)[a,b]	0.31	0.30 (0.06)[a,b]	0.32	<0.001
Ventral diencephalon, R	0.22 (0.03)[a]	0.22	0.24 (0.03)	0.24	0.29 (0.06)[a,b]	0.30	0.29 (0.07)[a,b]	0.31	<0.001
Ventral diencephalon, L	0.22 (0.05)	0.21	0.24 (0.04)	0.24	0.30 (0.06)[a,b]	0.31	0.29 (0.09)[a,b]	0.32	<0.001
Brainstem	0.23 (0.04)	0.23	0.23 (0.04)	0.23	0.30 (0.05)[a,b]	0.31	0.29 (0.07)[a,b]	0.31	<0.001
Cerebellum, R	0.12 (0.05)	0.12	0.15 (0.05)	0.14	0.23 (0.07)[a,b]	0.24	0.24 (0.06)[a,b]	0.25	<0.001
Cerebellum, L	0.16 (0.06)	0.17	0.16 (0.06)	0.17	0.24 (0.07)[a,b]	0.25	0.24 (0.08)[a,b]	0.26	<0.001
Nodal path length									
Subcortical									
Hippocampus, R	0.016 (0.003)	0.015	0.014 (0.002)	0.014	0.017 (0.004)[a]	0.017	0.017 (0.002)[a]	0.017	<0.001

[a]Significantly different from male HC.
[b]Significantly different from male Fxpc.

In female fXPCs, CC in the left superior parietal cortex correlated positively with the attentionally demanding counting response time in our Enumeration task, even after accounting for CGG repeats. This indicates that increased local network segregation was related to poorer performance. Also, several more relationships consistent with our hypotheses showed statistical trends towards correlations in the adult female fXPCs between key perceptual and motor brain regions and measures of those same cognitive functions. Specifically, CC in the left precuneus showed a positive relationship with response time on the subitizing component of the Enumeration task. There is now a large literature linking many components of the medial and lateral inferior parietal lobes, including the

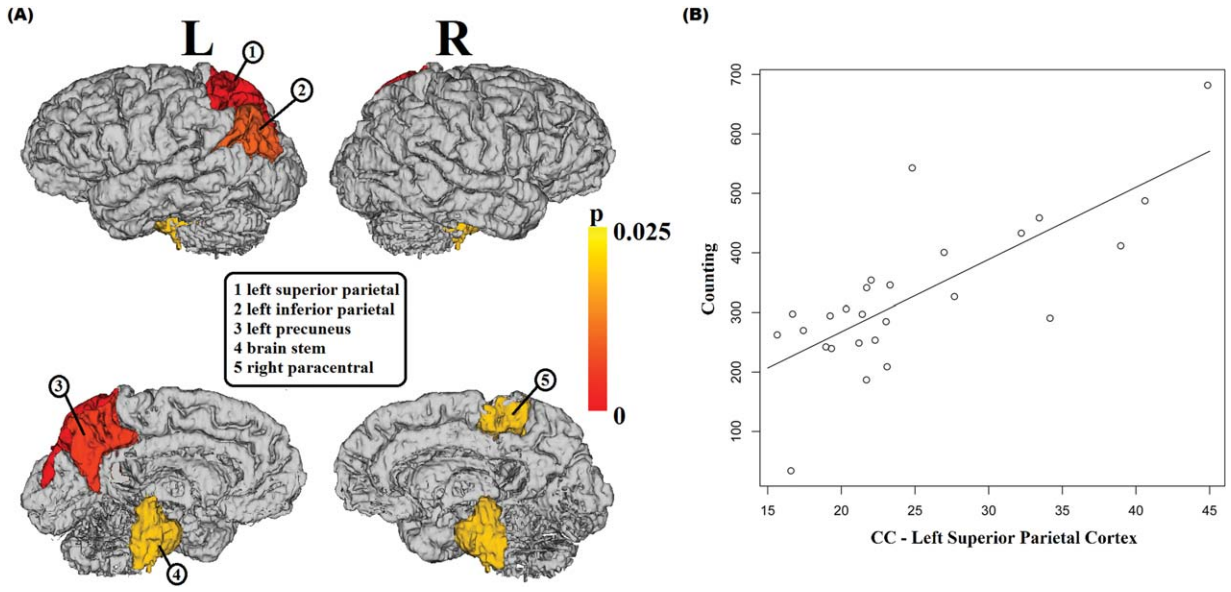

Figure 3.

A: Surface rendering of brain regions showing significant correlations with cognitive tasks. **B**: Association between counting on the Enumeration task and the CC in the left superior parietal cortex in female fXPCs ($r = 0.75$, $P < 0.001$).

precuneus, to a range of attentional, comparative, and quantitative cognitive functions [Ansari, 2008; Cohen Kadosh et al., 2005; Shuman and Kanwisher, 2004]. Of course, such regions do not act alone and are part of well-described processing circuits that have critical interconnections with frontal, occipital, and temporal cortices. Thus a possible "overlocalization" of the most central processing nodes might impede information transfer and slow performance on such tasks. The same female fXPCs participants also showed a trend toward a negative relationship between local network integration in the brain stem (as measured by nodal efficiency) and manual motor reaction time, and between the local network integration in the right paracentral cortex (as measured by nodal path length) and oral reaction time. These relationships are consistent with the connectivity of the motor system; the brain stem has direct connections with the motor cortex and the paracentral cortex includes the supplementary motor area, which is a central component of the motor control system, particularly of internally generated movements.

By contrast, in male fXPCs, we did not see any significant associations between nodal measures and task performance. The lack of significant association results for the male fXPCs was most likely due to the much smaller sample of that gender. Taken as whole, these results provide important hypotheses regarding neural biomarkers that need to be evaluated by future larger studies. Together the trends in our correlation data suggest that larger sample studies in the future might be able to identify very sensitive biomarkers in motor and perceptual networks for cognitive functions that are consistent with well-known neurological symptoms of FXTAS and milder forms of neurodegeneration in the fragile X spectrum.

Lastly, we note that our results additionally support notable gender differences, regardless of their premutation status. Indeed, in our secondary analyses, female participants exhibited lower global network clustering regardless of the diagnostic group. Locally, we also found widespread higher local efficiency and/or lower local clustering in both groups of female participants. Our findings are in general consistent with existing literature on gender differences of brain connectome, supporting that women, on average, show greater overall cortical connectivity and the underlying organization of their cortical networks tends to be more efficient, both locally and globally [Gong et al., 2009; Yan et al., 2011].

CONCLUSION

Here, we present the first brain connectome study in both male and female carriers of the fragile X premutation allele relative to healthy controls. Our results suggest that this approach has considerable potential for sensitively detecting dose-modulated brain changes in relatively young, non-FXTAS fXPC. This represents novel findings in that both groups appear typically functioning not only behaviorally but also with respect to IQ, though males as a group do more poorly on some tasks than do HCs [Wong et al., 2012]. Thus, we argue that the ability to detect such subtle differences should be considered as an important approach, which in future studies may enable us to further discover possible neurobehavioral connectome biomarkers for detecting preclinical brain change in the fXPC spectrum.

ACKNOWLEDGMENTS

The NIH had no further role in study design; in the collection, analysis, and interpretation of data; in the writing of the report; and in the decision to submit the article for publication. The authors thank the participants who made this work possible.

REFERENCES

Ajilore O, Lamar M, Kumar A (2014): Association of brain network efficiency with aging, depression, and cognition. Am J Geriatr Psychiatry 22:102–110. doi: 10.1016/j.jagp.2013.10.004.

Ansari D (2008): Effects of development and enculturation on number representation in the brain. Nat Rev Neurosci 9:278–291.

Barnea-Goraly N, Eliez S, Hedeus M, Menon V, White CD, Moseley M, Reiss AL (2003): White matter tract alterations in fragile X syndrome: Preliminary evidence from diffusion tensor imaging. Am J Med Genet B Neuropsychiatr Genet 118B:81–88.

Bourgeois JA, Coffey SM, Rivera SM, Hessl D, Gane LW, Tassone F, Greco C, Finucane B, Nelson L, Berry-Kravis E, Grigsby J, Hagerman PJ, Hagerman RJ (2009): A review of fragile X premutation disorders: Expanding the psychiatric perspective. J Clin Psychiatry 70:852–862.

Brunberg JA, Jacquemont S, Hagerman RJ, Berry-Kravis EM, Grigsby J, Leehey MA, Tassone F, Brown WT, Greco CM, Hagerman PJ (2002): Fragile X premutation carriers: Characteristic mr imaging findings of adult male patients with progressive cerebellar and cognitive dysfunction. AJNR Am J Neuroradiol 23:1757–1766.

Bullmore E, Sporns O (2009): Complex brain networks: Graph theoretical analysis of structural and functional systems. Nat Rev Neurosci 10:186–198.

Cohen Kadosh R, Henik A, Rubinsten O, Mohr H, Dori H, van de Ven V, Zorzi M, Hendler T, Goebel R, Linden DE (2005): Are numbers special? The comparison systems of the human brain investigated by fmri. Neuropsychologia 43:1238–1248.

Dijkstra EW (1959): A note on two problems in connexion with graphs. Numer Math 1:269–271.

GadElkarim JJ, Schonfeld D, Ajilore O, Zhan L, Zhang AF, Feusner JD, Thompson PM, Simon TJ, Kumar A, Leow AD (2012): A framework for quantifying node-level community structure group differences in brain connectivity networks. Med Image Comput Comput Assist Interv 15:196–203.

Garcia-Arocena D, Hagerman PJ (2010): Advances in understanding the molecular basis of fxtas. Hum Mol Genet 19:R83–89.

Gong G, Rosa-Neto P, Carbonell F, Chen ZJ, He Y, Evans AC (2009): Age-and gender-related differences in the cortical anatomical network. J Neurosci 29:15684–15693.

Goodrich-Hunsaker NJ, Wong LM, McLennan Y, Srivastava S, Tassone F, Harvey D, Rivera SM, Simon TJ (2011a): Young

adult female fragile X premutation carriers show age- and genetically-modulated cognitive impairments. Brain Cogn 75: 255–260.

Goodrich-Hunsaker NJ, Wong LM, McLennan Y, Tassone F, Harvey D, Rivera SM, Simon TJ (2011b): Adult female fragile X premutation carriers exhibit age- and cgg repeat length-related impairments on an attentionally based enumeration task. Front Hum Neurosci 5:63.

Goodrich-Hunsaker NJ, Wong LM, McLennan Y, Tassone F, Harvey D, Rivera SM, Simon TJ (2011c): Enhanced manual and oral motor reaction time in young adult female fragile X premutation carriers. J Int Neuropsychol Soc 17:746–750.

Greco CM, Berman RF, Martin RM, Tassone F, Schwartz PH, Chang A, Trapp BD, Iwahashi C, Brunberg J, Grigsby J, Hessl D, Becker EJ, Papazian J, Leehey MA, Hagerman RJ, Hagerman PJ (2006): Neuropathology of fragile X-associated tremor/ataxia syndrome (FXTAS). Brain 129:243–255.

Griffa A, Baumann PS, Thiran JP, Hagmann P (2013): Structural connectomics in brain diseases. Neuroimage 80:515–526.

Haas BW, Barnea-Goraly N, Lightbody AA, Patnaik SS, Hoeft F, Hazlett H, Piven J, Reiss AL (2009): Early white-matter abnormalities of the ventral frontostriatal pathway in fragile X syndrome. Dev Med Child Neurol 51:593–599.

Hagerman PJ (2008): The fragile X prevalence paradox. J Med Genet 45:498–499.

Hagerman PJ, Hagerman RJ (2004): The fragile-X premutation: A maturing perspective. Am J Hum Genet 74:805–816.

Hagerman RJ, Leavitt BR, Farzin F, Jacquemont S, Greco CM, Brunberg JA, Tassone F, Hessl D, Harris SW, Zhang L, Jardini T, Gane LW, Ferranti J, Ruiz L, Leehey MA, Grigsby J, Hagerman PJ (2004): Fragile-X-associated tremor/ataxia syndrome (FXTAS) in females with the FMR1 premutation. Am J Hum Genet 74:1051–1056.

Hashimoto R, Srivastava S, Tassone F, Hagerman RJ, Rivera SM (2011): Diffusion tensor imaging in male premutation carriers of the fragile X mental retardation gene. Mov Disord 26:1329–1336.

Hessl D, Rivera S, Koldewyn K, Cordeiro L, Adams J, Tassone F, Hagerman PJ, Hagerman RJ (2007): Amygdala dysfunction in men with the fragile X premutation. Brain 130:404–416.

Hocking DR, Kogan CS, Cornish KM (2012): Selective spatial processing deficits in an at-risk subgroup of the fragile X premutation. Brain Cogn 79:39–44.

Jacquemont S, Hagerman RJ, Leehey MA, Hall DA, Levine RA, Brunberg JA, Zhang L, Jardini T, Gane LW, Harris SW, Herman K, Grigsby J, Greco CM, Berry-Kravis E, Tassone F, Hagerman PJ (2004a): Penetrance of the fragile X-associated tremor/ataxia syndrome in a premutation carrier population. JAMA 291:460–469.

Jacquemont S, Farzin F, Hall D, Leehey M, Tassone F, Gane L, Zhang L, Grigsby J, Jardini T, Lewin F, Berry-Kravis E, Hagerman PJ, Hagerman RJ (2004b): Aging in individuals with the FMR1 mutation. Am J Ment Retard 109:154–164.

Kim S-Y, Hashimoto R-i, Tassone F, Simon TJ, Rivera SM (2013): Altered neural activity of magnitude estimation processing in adults with the fragile X premutation. J Psychiatric Res 47: 1909–1916.

Kogan CS, Boutet I, Cornish K, Zangenehpour S, Mullen KT, Holden JJ, Der Kaloustian VM, Andermann E, Chaudhuri A (2004): Differential impact of the FMR1 gene on visual processing in fragile X syndrome. Brain 127:591–601.

Koldewyn K, Hessl D, Adams J, Tassone F, Hagerman PJ, Hagerman RJ, Rivera SM (2008): Reduced hippocampal activation during recall is associated with elevated FMR1 mrna and psychiatric symptoms in men with the fragile X premutation. Brain Imaging Behav 2:105–116.

Leow A, Ajilore O, Zhan L, Arienzo D, GadElkarim J, Zhang A, Moody T, Van Horn J, Feusner J, Kumar A, Thompson P, Altshuler L (2013): Impaired inter-hemispheric integration in bipolar disorder revealed with brain network analyses. Biol Psychiatry 73:183–193.

MacLeod LS, Kogan CS, Collin CA, Berry-Kravis E, Messier C, Gandhi R (2010): A comparative study of the performance of individuals with fragile X syndrome and FMR1 knockout mice on hebb-williams mazes. Genes Brain Behav 9:53–64.

Rubinov M, Sporns O (2010): Complex network measures of brain connectivity: Uses and interpretations. Neuroimage 52:1059–1069.

Schneider A, Hagerman RJ, Hessl D (2009): Fragile X syndrome - from genes to cognition. Dev Disabil Res Rev 15:333–342.

Shuman M, Kanwisher N (2004): Numerical magnitude in the human parietal lobe; tests of representational generality and domain specificity. Neuron 44:557–569.

Sulkowski GM, Kaufman LM (2008): Oculomotor abnormalities in a patient with fragile X-associated tremor/ataxia syndrome. J AAPOS 12:195–196.

Tassone F, Pan R, Amiri K, Taylor AK, Hagerman PJ (2008): A rapid polymerase chain reaction-based screening method for identification of all expanded alleles of the fragile X (FMR1) gene in newborn and high-risk populations. J Mol Diagn 10: 43–49.

Verkerk AJ, Pieretti M, Sutcliffe JS, Fu YH, Kuhl DP, Pizzuti A, Reiner O, Richards S, Victoria MF, Zhang FP, et al. (1991): Identification of a gene (fmr-1) containing a cgg repeat coincident with a breakpoint cluster region exhibiting length variation in fragile X syndrome. Cell 65:905–914.

Wang JY, Hessl DH, Hagerman RJ, Tassone F, Rivera SM (2012): Age-dependent structural connectivity effects in fragile X premutation. Arch Neurol 69:482–489.

Wechsler D (1997): Wechsler Adult Intelligence Scale–Third Edition (WAIS-III®). Harcourt Assessment: San Antonio, TX.

Wechsler D (1999): Wechsler Abbreviated Scale of Intelligence (WASI). Harcourt Assessment: San Antonio, TX.

Wig GS, Schlaggar BL, Petersen SE (2011): Concepts and principles in the analysis of brain networks. Ann N Y Acad Sci USA 1224:126–146.

Wong LM, Goodrich-Hunsaker NJ, McLennan Y, Tassone F, Harvey D, Rivera SM, Simon TJ (2012): Young adult male carriers of the fragile X premutation exhibit genetically modulated impairments in visuospatial tasks controlled for psychomotor speed. J Neurodev Disord 4:26.

Yan C, Gong G, Wang J, Wang D, Liu D, Zhu C, Chen ZJ, Evans A, Zang Y, He Y (2011): Sex-and brain size–related small-world structural cortical networks in young adults: A dti tractography study. Cereb Cortex 21:449–458.

Xia M, He Y (2011): Magnetic resonance imaging and graph theoretical analysis of complex brain networks in neuropsychiatric disorders. Brain Connect 1:349–365.

Zhu W, Wen W, He Y, Xia A, Anstey KJ, Sachdev P (2012): Changing topological patterns in normal aging using large-scale structural networks. Neurobiol Aging 33:899.